Classical and Quantum simulation of Extreme Plasma Physics

Óscar Amaro
oscar.amaro@tecnico.ulisboa.pt

Instituto Superior Técnico, Lisboa, Portugal

December 2021

Abstract

Recent advances in laser technology will soon allow explorations into new regimes of electrodynamics, and possibly lead to the discovery of new physics. One of the most promising experiments to observe signals from Quantum Electrodynamics is a frontal electron-laser scattering. Accurate estimates of observables in these experiments usually require *ab-initio* simulations (e.g. Particle-in-cell codes with Monte Carlo routines), which are computationally expensive. Furthermore, analytical models usually restrict to highly idealized setups, like the plane wave, which do not map well to experiments. In this work we propose a new semi-analytical approach to focused laser scattering, which allows extending scaling laws originally derived for plane wave to realistic scenarios. This method allows accurate estimations and optimization of the positron yield when the laser spotsize is a free parameter.

In a parallel line of work we investigate the potential use of Quantum Computing (QC) to model extreme plasmas. This new information processing paradigm promises significant speedups for certain classes of problems in the coming decades. Although already somewhat mature in the areas adjacent to Quantum Mechanics, QC is still in its cradle regarding Plasma Physics. We highlight some scenarios where new quantum algorithms could be developed.

Keywords: Plasma; Radiation reaction; Quantum Electrodynamics; Compton Scattering; Pair Production; PIC simulations; High Performance Computing; Quantum Computing; Variational Algorithm

1. Pair Production in Electron-Laser Scattering

1.1. Introduction

Plasma Physics is the field of many-body Physics dealing with long-range electromagnetic interactions. A plasma is a state of matter in which charged particles are mostly free (few bound atoms or molecules) and collective phenomena dominate (as opposed to inter-particle collisions) and is the most abundant form of ordinary matter in the universe. They are fundamental to understanding fusion in stars, turbulence, and the origin of magnetic fields in space.

Recent progress in laser technology and particle acceleration will allow experiments in ultrarelativistic and quantum electrodynamical processes in plasmas [1]. At the same time, the dynamics of astrophysical objects such as pulsars [2] and jets from and accretion disks around black holes depend heavily on Plasma Physics [3, 4]. These phenomena are part of the subfield of Extreme Plasma Physics, whose simulations are numerically heavy due to their inherent nonlinearity. It would, therefore, greatly benefit from new algorithm development, namely in the quantum paradigm.

In an intense electromagnetic background, charged particles obtain relativistic velocities and emit energetic photons. A fraction of these photons decays into electron-positron pairs, which can themselves be accelerated by the fields and radiate new photons [5, 6]. These effects can then lead to quantum vacuum polarization, light-by-light scattering, vacuum birefringence, four-wave mixing, and high order harmonic generation from the vacuum.

Although Quantum Electrodynamics (QED) is one of the most thoroughly verified physical theories for elementary processes, the rich dynamics arising from plasmas' collective behavior is still poorly understood. It has been suggested that energy densities similar to those required to observe these effects can be re-created in the laboratory by using counter-propagating intense laser pulses [1]. This has led to the study of variations of this configuration using kinetic simulations[7, 8, 9, 10].

Because the required laser intensities ($I \sim 10^{24}$ Wcm^{-2}) are still beyond what is currently

possible with the latest technology, it is not easy to study the highly nonlinear dynamics of extreme plasmas.

The technique of LWFA [11] consists of sending a laser pulse through a plasma and using the EM wake generated to accelerate electrons in very short distances. This allows having energetic beams and intense lasers at the same laboratory and study electron-laser scattering.

Currently, conventional accelerators still allow better quality and control than LWFA because its technology is more mature. However, as LWFA becomes a standard scientific tool, laboratories can become increasingly more compact and use a single laser system for acceleration and scattering.

Before lasers become sufficiently intense to generate dense e^+e^- pair plasmas from light, a head-on collision between a pulsed laser and a very energetic electron beam can allow us to generate dilute e^+e^- beams by applying currently available technology [12]. Research on stochastic effects in radiation reaction is also expected to benefit from the laser-electron scattering experiments [13, 14, 15, 16, 17], with new ways to infer the peak laser intensity at the interaction point [18, 19] and probing the transition from the classical to the quantum-dominated laser-electron interaction. Two all-optical experiments have shown the electron slowdown due to radiation reaction [20, 21], but were not able to discriminate between different theoretical descriptions of radiation reaction.

We anticipate that the near-future facilities (e.g. ELI, Apollon , CoReLS , FACET-II [22], LUXE [23], EXCELS, ZEUS) are to probe electron-positron pair production, covering several different regimes of interaction. This manuscript focuses on head-on laser-electron scattering that maximizes the strength of the electric field in the electron rest frame. This is the first planned experiment in most of the aforementioned facilities, and we aim to improve the current predictive capabilities for positron creation.

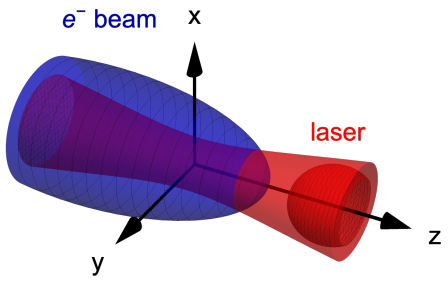

Figure 1: Scattering of an relativistic electron beam (blue) and a counter-propagating laser pulse (red).

Due to the inherent non-linearity of the Breit-Wheeler pair production, there is no general roadmap on what would be an optimal strategy to obtain the highest possible positron yield using any given laser system. If the laser is assumed to be a plane wave (adequate when the laser is much wider than the interacting beam), the analytical predictions state that the best strategy would be to use the highest conceivable laser intensity. Therefore it is tempting to conclude that the laser should be focused on the smallest attainable focal spot. Our work shows that this strategy may not always be optimal, as there is a trade-off between the high laser intensity and the size of the interaction volume.

This work has resulted in a paper [24], submitted to New Journal of Physics.

1.2. QED phenomena

In QED theory, the threshold field for which the vacuum becomes unstable for pair creation is $E_{\rm cr} = 1.326 \times 10^{18}$ Vm^{-1}. Above this value the field can no longer be described classically, and we should expect a significant production of electron-positron pairs [25]. The invariant parameter that quantifies the effects of radiation reaction on the trajectories of leptons is $\chi_e = |F^{\mu\nu}p_\nu|/(E_{\rm cr}m)$, where $F^{\mu\nu}$ is the EM field tensor and p_ν is the corresponding particle four-momentum. The larger its value, the greater the differences between the quantum and classical predictions of radiation emission. There is an analogous quantity for photons χ_γ.

The rate of photon emission by a lepton is given by

$$\frac{\mathrm{d}^2P}{\mathrm{d}t\ \mathrm{d}\chi_\gamma} = \frac{\alpha mc^2}{\sqrt{3}\pi\hbar\gamma\chi_e}\left[\left(1-\xi+\frac{1}{1-\xi}\right)K_{2/3}(\tilde{\chi}) - \int_{\tilde{\chi}}^{\infty} K_{1/3}(x)\mathrm{d}x\right] \tag{1}$$

where $\tilde{\chi} = 2\xi/\left(3\chi_e(1-\xi)\right), \xi = \chi_\gamma/\chi_e$, γ is the lepton's Lorentz factor. Analogously, photons can decay into electron-positron pairs in the presence of extreme fields according to

$$\frac{\mathrm{d}^2P}{\mathrm{d}t\ \mathrm{d}\chi_e} = \frac{\alpha m^2c^4}{\sqrt{3}\pi\hbar\omega\chi_\gamma}\left[\left(\frac{\xi^+}{\xi^-}+\frac{\xi^-}{\xi^+}\right)K_{2/3}(\tilde{\chi}) + \int_{\tilde{\chi}}^{\infty} K_{1/3}(x)\mathrm{d}x\right] \tag{2}$$

where $\tilde{\chi} = 2/\left(3\chi_\gamma\xi^+\xi^-\right)$, $\xi^+ = \chi_e/\chi_\gamma = 1-\xi^-$, and ω is the photon frequency. These rates can be included in Monte-Carlo codes in order to self-consistently simulate the evolution of an extreme plasma.

1.3. Pair Production in a Plane Wave

The simplest description of a laser pulse is a plane wave with a temporal envelope. Such a wave is fully described by the wavelength λ, a pulse duration τ, and the normalized vector potential a_0, which relates to the intensity through $a_0 = 0.855\sqrt{I[10^{18}\ \mathrm{W/cm^2}]}\lambda[\mu\mathrm{m}]$ (for linearly polarized lasers). As a relativistic electron interacts with the strong electromagnetic wavepacket, it emits

high-energy photons that can decay into electron-positron pairs through the Breit-Wheeler mechanism [26].

In the plane wave approximation, the total number of new pairs per interacting electron can be estimated if we know the initial electron energy $\gamma_0 mc^2$ (where γ_0 is the electron Lorentz factor, m the electron mass and c is the speed of light), and the laser parameters (peak a_0, central wavelength λ and pulse duration τ, which is defined as the full width at half maximum of the laser intensity). The total number of pairs is then given by [27]:

$$N_+^{\mathrm{PW}}(\gamma_0, a_0, \lambda, \tau) \simeq 3\sqrt{\frac{\pi}{2}} P_\pm(\omega_c)\ \chi_{\mathrm{c,rr}} \frac{(\gamma_0 mc^2 - \hbar\omega_c)^2}{\hbar\gamma_0 mc^2}\ \left.\frac{\mathrm{d}N_\gamma}{\mathrm{d}\omega}\right|_{\omega=\omega_c} \tag{3}$$

The first term $P_\pm(\omega_c)$ represents the probability of a photon of frequency ω_c decaying during interaction with the laser pulse; the second is the recoiled $\chi_{\mathrm{c,rr}}$ which accounts for the radiation reaction on the beam electrons and the final term $\mathrm{d}N_\gamma/\mathrm{d}\omega$ is the value of the emitted photon distribution at $\omega = \omega_c$.

According to this model, all positrons are generated from photons with a critical frequency ω_c, and there is no feedback by the produced pairs on the photon spectra (in other words, there is only one generation of secondary particles). Furthermore, the model assumes a semi-classical equation of motion of the electrons as they lose energy through the emission of radiation and uses the locally constant field and rigid-beam approximations. This allows an implicit calculation of the laser phase ϕ_c at which χ_e is maximized, which is later used to estimate the emitted photon spectrum and consequently the number of created pairs.

1.4. Beyond Plane Wave

Let us now consider a diffraction-limited laser pulse illustrated in figure 1. The maximum laser intensity an individual particle within the electron beam interacts with depends on two geometrical factors: the transverse offset from the laser axis compared to the laser spotsize and the initial longitudinal position that affects the temporal synchronization of the interaction. While interacting with a Gaussian laser pulse, electrons far from the focus interact with a lower average (and peak) field, which must be taken into account. The model assumed for this type of focused laser is

$$a_{0,\mathrm{eff}} = \frac{a_0}{\sqrt{1+(z/z_R)^2}} \exp\left(-\frac{(x^2+y^2)/W_0^2}{1+(z/z_R)^2}\right) \tag{4}$$

where W_0 is the laser spotsize, $z_R \equiv \pi W_0^2/\lambda$ is the Rayleigh range.

The electron encounters the peak of the laser pulse at time t in an (x, y, z) point of configuration space which defines the maximum field felt by this particle. We can therefore assign an effective vector potential $a_{0,\mathrm{eff}}(t, x, y, z)$ that corresponds to the maximum laser intensity the particle experiences during the interaction.

We define an equivalent distribution of beam particles according to the maximum intensity they interact with during the scattering. This intensity is identified through the maximum instantaneous vector potential associated with an individual beam particle as $a_{0,\mathrm{eff}}$. In the case of a plane wave interaction, there is no defocusing, and particles always interact with the same intensity, regardless of where or when they overlap with the peak of the laser ($a_{0,\mathrm{eff}} = a_0$, and the equivalent distribution, in this case, would be a dirac Delta function). For a more general case, by considering a corrected $a_{0,\mathrm{eff}}$ for each particle, we can apply the equations already derived for a plane wave (equation 3), and then integrate over the distribution function in $a_{0,\mathrm{eff}}$ to obtain the total yield of positrons in the laser-electron scattering. This calculation can be performed either by sampling the distribution function numerically or by performing an analytical integration over the configuration space.

In Ref. [27] the authors calculate the total number of positrons by analytically and numerically integrating the scaling law for the plane wave in full coordinate space (x, y, z). Our approach allows to make this procedure shorter and applicable to different beam shapes and sizes. After deriving the distribution of particles $\mathrm{d}N/\mathrm{d}a_{0,\mathrm{eff}}$, a 1-dimensional integration in $a_{0,\mathrm{eff}}$-space is enough to make predictions on the total number of expected positrons (or some other relevant quantity).

Our approach is to first obtain a distribution of the interacting particles according to their $a_{0,\mathrm{eff}}$. For every bin in this distribution $\mathrm{d}N(a_{0,\mathrm{eff}})/\mathrm{d}a_{0,\mathrm{eff}}$ one can calculate the contribution for pair production using $N_+^{\mathrm{PW}}(\gamma_0, a_{0,\mathrm{eff}}, \lambda, \tau)$. This method is cost-effective because it eliminates the need to perform multiple variable integration in configuration space.

The problem can be addressed using cylindrical coordinate system (ρ, ϕ, z), centered at the laser focus. For a Gaussian laser beam (in the paraxial approximation), the configuration space can be mapped according to the laser intensity isosurfaces shown in figure 2, that do not depend on the coordinate ϕ. For simplicity, let us first assume that the electron beam is a cylinder with a constant density n_b. Each particle meets the laser beam at a different point of space, and is assigned $a_{0,\mathrm{eff}}(\rho, z)$, where ρ and z are its coordinates at the instant of time when it is synchronised with the peak of the laser. Performing a one-to-one mapping to the new coordinates of a flat-top relativistic beam in counter-propagation with the laser, the beam den-

sity in the new coordinates doubles and the length halves because the laser-electron crossing occurs at twice the speed of light. The number of particles $\mathrm{d}N_b(a_{0,\mathrm{eff}})$ with $a_{0,\mathrm{eff}}$ that falls in the interval $[a_{0,\mathrm{eff}}, a_{0,\mathrm{eff}} + \mathrm{d}a_{0,\mathrm{eff}}]$ can then be estimated to be $\mathrm{d}N_b(a_{0,\mathrm{eff}})/\mathrm{d}a_{0,\mathrm{eff}} = 2n_b\ \mathrm{d}V/\mathrm{d}a_{0,\mathrm{eff}}$, where $\mathrm{d}V$ is the volume between two adjacent isosurfaces associated with $a_{0,\mathrm{eff}}$ and $a_{0,\mathrm{eff}} + \mathrm{d}a_{0,\mathrm{eff}}$. Due to the geometry of the problem, this expression can be transformed to the following:

$$\frac{\mathrm{d}N_b(a_{0,\mathrm{eff}})}{\mathrm{d}a_{0,\mathrm{eff}}} = \int_S \frac{2n_b\ \mathrm{d}S}{||\nabla a_{0,\mathrm{eff}}||} \tag{5}$$

where the surface element $\mathrm{d}S = \rho\sqrt{\mathrm{d}\rho^2 + dz^2}\ \mathrm{d}\phi = \rho\sqrt{1 + (\partial\rho/\partial z)^2}\ \mathrm{d}z\ \mathrm{d}\phi$ is calculated at the isosurface that is by definition perpendicular to the gradient of the vector potential given by $||\nabla a_{0,\mathrm{eff}}|| = \sqrt{(\partial a_{0,\mathrm{eff}}/\partial\rho)^2 + (\partial a_{0,\mathrm{eff}}/\partial z)^2}$.

Letting beam plasma density vary in space $n_b(\vec{r})$ allows considering cases of short or long, wide or narrow beams, including non-ideal spatio-temporal synchronization with the laser. It is worth noting that even a point-particle interaction with a Gaussian beam is not equivalent to a plane wave approximation unless the particle is in perfect temporal synchronization with the laser pulse.

An alternative way to obtain the distribution of particles in $a_{0,\mathrm{eff}}$ is to numerically sample the electron beam density $n_b(r, \theta, \phi)$ in space (the "sampling" method). The sampled distribution function can be directly binned into a histogram according to the maximum value of a_0 each section interacts with.

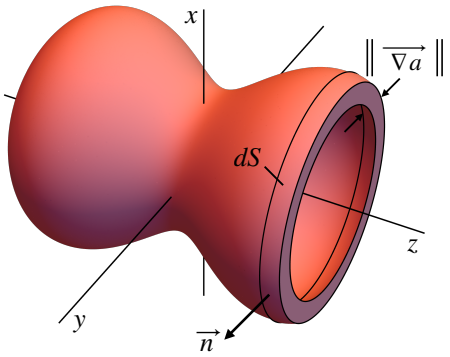

Figure 2: A volume element between two isosurfaces of the effective normalized vector potential $a_{0,\mathrm{eff}}$. The volume element contains all the points where particles experience the peak a_0 within the interval $[a_{0,\mathrm{eff}}, a_{0,\mathrm{eff}} + \mathrm{d}a_{0,\mathrm{eff}}]$.

In this work we consider 3 new types of geometries beyond the plane wave setup (see Figure 3).

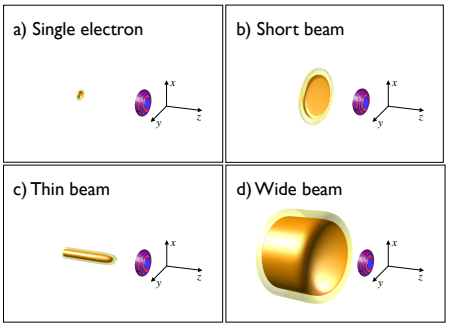

Figure 3: Geometries considered in this Thesis: point-like, short, thin, and wide beams.

1.5. Synchronized scattering for a Wide beam

In the case of a wide electron beam ($R \gg W_0$), is is possible to derive an analytical distribution of particles in $a_{0,\mathrm{eff}}$

$$\frac{\mathrm{d}N_b}{\mathrm{d}a_{0,\mathrm{eff}}} = \begin{cases} \dfrac{4\pi\ n_b\ W_0^2\ z_R}{a_{0,\mathrm{eff}}} \dfrac{\sqrt{a_0^2 - a_{0,\mathrm{eff}}^2}}{3a_{0,\mathrm{eff}}} \left(2 + \left(\dfrac{a_0}{a_{0,\mathrm{eff}}}\right)^2\right), & a_{0,\mathrm{eff}} \geq a_z \\ \dfrac{4\pi\ n_b\ W_0^2\ z_R}{a_{0,\mathrm{eff}}} \dfrac{L}{4z_R} \left(1 + \left(\dfrac{L}{4z_R}\right)^2\right), & a_{0,\mathrm{eff}} < a_z \end{cases} \tag{6}$$

where $a_z = a_0/\sqrt{1 + (z/z_R)^2}$.

In figure 4 this distribution is plotted for different beam lengths.

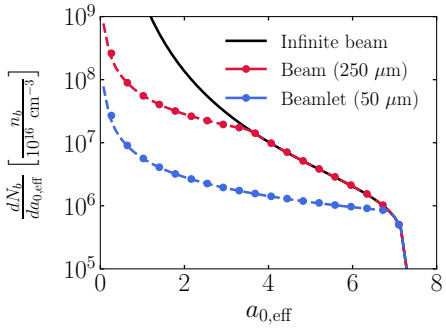

Figure 4: Particle distribution in the geometry of a Wide beam: dot - sampling, dashed - analytical distribution. Several beam lengths were considered.

1.6. Unsynchronized scattering

In experiments, the timing of the scattering can suffer from parameter fluctuations in the laser system, such that the middle of the electron beam will cross the peak of the laser at a distance $\Delta_{\parallel}$ from the focus. This unsynchronization will break the symmetry assumed in the previous calculations, and in general lead to a lower average intensity felt by the particles. However, it is straightforward to extend the synchronized distributions to this new case, as illustrated in Figure 5.

Whereas before the boundaries of the electron beam were mapped to $z_- = -L/4$ and $z_+ = +L/4$, now they are shifted to $z_- = -L/4 + \Delta_\parallel$ and $z_+ = +L/4 + \Delta_\parallel$. The beam can be divided into two parts: the blue part on the left-hand side of the focal plane and the yellow part on the right-hand side of the focal plane. This can be interpreted as follows: the total distribution in $a_{0,\text{eff}}$ can be written as a sum of the distributions coming from the blue and the yellow sections of the beam. Each of these beams contributes with exactly half of the distribution function associated with a symmetrical (temporally synchronized) beam twice its size. This means we can reuse the distribution functions, modifying the beam lengths to $|z_-|$ and $|z_+|$. For a large temporal offset $\Delta_\parallel > L/4$, none of the beam particles interact with the laser in the focus (this is illustrated in figure 5 b)). In this case, we subtract the contribution of the blue beam from the contribution of the yellow beam.

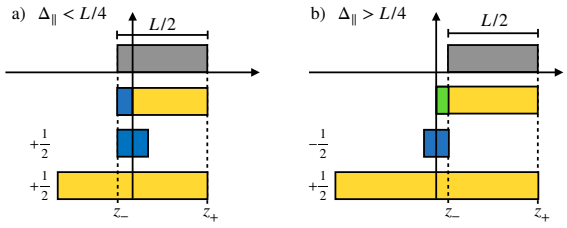

Figure 5: Geometrical approach to calculate the particle distribution in a unsynchronized scattering.

1.7. Optimal laser spotsize

When designing experiments to test the theory of plasma-QED, one of the goals is to maximize the number of positrons created, such that, in the end, the measured signal is large. To achieve this, the first idea would be to focus the laser on the smallest attainable focal spot (with all other parameters fixed). However, there will be a trade-off between the high laser intensity and the size of the interaction volume. With a short focus, the highest intensity region becomes small both transversely and longitudinally, which can reduce the number of seed particles that interact with the high intensity and the duration of this interaction. Using tight focusing also increases the number of particles that are not temporally synchronized with the laser pulse's peak at the focal plane and changes the effective angle of interaction due to the wavefront curvature.

To find the balance between the competing effects, we can first scan the possible values of the laser focusing and numerically compute the corresponding positron yield. From this, optimal spot sizes can be extracted (see Figure 6). The same procedure can be done with other parameters, such as the laser pulse duration. Ideally, these optimal values could be derived analytically. We can then recommend optimal experimental conditions for existing and future facilities. This would allow real-time parameter scans and easily check the positron production changes, for example, when upgrading one component of the system.

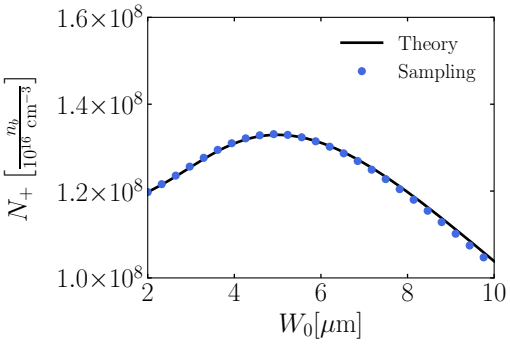

Figure 6: Positron yield variation with spot size. For each laser pulse energy there will be an optimal W_0 value.

1.8. Optimal parameters for laser facilities

This section covers the optimal focusing strategy for a wide range of laser parameters (in particular as a function of total energy content and pulse duration), as well as different electron beam energies. We assume that the electron beam is 200 μm long (flat-top longitudinal envelope) and has a Gaussian transverse shape. The electron beam is spatio-temporally synchronized with the laser (i.e., the center of the beam interacts with the laser peak at the focal plane, and they share the propagation axis). The transverse beam profile is Gaussian with $\sigma_x = 24.4$ μm and $\sigma_y = 29.6$ μm. The chosen on-axis beam density $n_b = 10^{16}$ cm^{-3} corresponds to the total beam charge of $Q_b = 2$ nC. The results can be scaled to other values for the central beam density by introducing a factor $n_b/10^{16}$ cm^{-3}. A specific laser system has a fixed total energy content, which for a Gaussian transverse profile is approximately given by $\varepsilon[\text{J}] \sim 2.1\times10^{-5}\ a_0^2\ (W_0/\lambda)^2\ \tau[\text{fs}]$. The laser intensity (proportional to a_0^2) is therefore inversely proportional to the square of the spot size W_0. As the number of pairs produced per interacting electron N_+^{PW} is a monotonously rising function of the effective a_0, and the number of seed electrons that would experience the high intensity is proportional to the size of the interaction volume $\sim W_0^2 z_R$, to obtain the highest possible number of positrons, one should strike the right balance between a high value of a_0 and a large W_0. In other words, there is a trade-off between using a short focal length to obtain the highest conceivable laser intensity and having a wider interaction volume where more seed electrons participate in the interaction.

What follows is a calculation of the optimal focal spot and the corresponding pair yield for lasers with energy below 1 kJ and relativistic particle beams

with energies lower or equal to 20 GeV. These values include what will soon be available in several experimental facilities (e.g. SLAC, HiBEF [28] or ELI [29]).

For each combination of the electron beam energy and the laser total energy content, we apply the analytical expression to calculate the effective a_0 distribution of the interacting particles. Then, we integrate the results numerically to find the optimal spotsize and maximum positron yield for this set of parameters.

Figure 7 summarizes the optimization results covering $\sim$ 1000 different parameter combinations, keeping the laser duration constant at 35 fs. For 10 GeV electrons and a 1 kJ laser, a maximum number of pairs is 10^9, which is obtained using $W_0 > 8$ μm. The FACET-II 13 GeV electron beam at SLAC could generate 4×10^8 pairs/shot if paired with a 300 J laser-focused to $W_0 = 5.7$ μm. The LUXE 17.5 GeV beam with the same laser parameters could produce 7×10^8 pairs per shot, using a slightly larger $W_0 = 6.8$ μm.

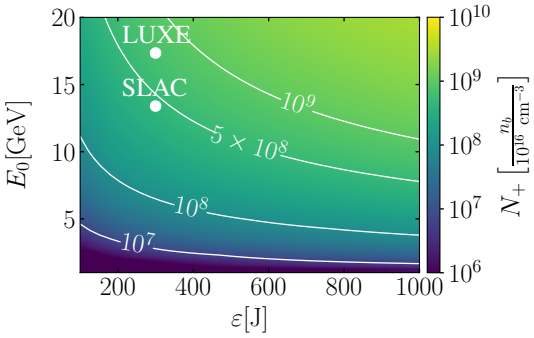

Figure 7: Iso-contours of the positron yield for various values of laser and electron energy.

2. Quantum Algorithms

2.1. Introduction

Quantum Computing is a new paradigm in performing calculations. It relies on the laws of quantum mechanics to process information in a non-classical manner and may offer advantages over standard techniques in some situations.

The idea of quantum computation, as suggested by Feynman [30], Manin and others, was primarily motivated by the problem of quantum simulation. There are already quantum machines capable of simulating small molecules and other systems, which may accelerate progress in fundamental science and industrial applications.

We are now in the so-called Noisy Intermediate-Scale Quantum (NISQ) era [31], in which quantum hardware still faces many issues on performance, limiting the number of qubits and the number of quantum operations allowed in a single computation. Until error-corrected codes and better hardware are developed, algorithms need to be designed considering these constraints.

The development of quantum algorithms in Physics has been mainly motivated by fundamental Quantum Mechanics, Quantum Chemistry, and Condensed Matter problems. Only recently has there been an interest in developing quantum versions of algorithms used in Plasma Physics, leveraging the extensive know-how of this scientific community. This late development of the field is partly justified by the inherent difficulty of solving nonlinear problems in quantum computers and the recent progress on quantum hardware.

2.2. Fokker Planck

The Fokker-Planck equation is a stochastic differential equation and is used in areas such as in laser-plasma interaction, namely to kinetically model collision between plasma species. An important application is in simulating the energy loss of an electron beam as it interacts with electromagnetic fields [13, 14]. In this case, the particle distribution evolves through

$$\frac{\mathrm{d}}{\mathrm{d}t} f(t, \vec{p}) = \frac{\partial}{\partial p_l} \left[A_l f + \frac{1}{2} \frac{\partial}{\partial p_k} \left(B_{lk} f \right) \right] \qquad (7)$$

with $A_l = \int q_l w(\vec{p}, \vec{q}) \mathrm{d}^3\vec{q}$, $\quad B_{lk} = \int q_l q_k w(\vec{p}, \vec{q}) \mathrm{d}^3\vec{q}$, the drift and diffusion coefficients respectively, and $w(\vec{p}, \vec{q})\ \mathrm{d}^3\vec{p}$ is the probability per unit time of momentum change of the electron $\vec{p} \to \vec{p} - \vec{q}$, with $\vec{q}$ the momentum of the photon.

In [15] the authors apply the Fokker Planck equation to simulate an electron beam that looses energy as it emits photons. As electrons propagate perpendicularly to a constant magnetic field B, this is effectively a 1D problem. The change in momentum for a single particle then becomes

$$\mathrm{d}\gamma(t) = -S(\chi)\ \mathrm{d}t + \sqrt{R(\chi, \gamma)}\ \mathrm{d}W \qquad (8)$$

where $S(\chi)$ and $R(\chi, \gamma)$ are related to the QED rate of photon emission, $\chi \propto \gamma\ B$ and $\mathrm{d}W$ is a Wiener motion.

There has been some progress in developing quantum algorithms to solve stochastic differential equations, mainly motivated by finance, physics and biology. In [32] the authors apply a variational method to solve equations of the type

$$\mathrm{d}X(t) = \mu(X(t), t)\ \mathrm{d}t + \sigma(X(t), t)\ \mathrm{d}W \qquad (9)$$

where $\mu(X(t), t)\sigma(X(t), t)$ are real-valued functions of time and coordinate, and W is a Brownian motion. This is exactly of the form of 8.

Applying this quantum algorithm to the Fokker-Planck equation in the context of Extreme Plasma Physics will be left for future work.

2.3. Plasma-QED Kinetic equations

In the regime where the fraction of the lepton's energy change is close to unity $\mathrm{d}\gamma \leq \gamma$, the Fokker-Planck equation is no longer adequate, and one needs to use the linear Boltzmann equation. Whereas the previous method only connects neighbour grid cells in momentum space, the full Boltzmann equation is dense in the sense that there is a finite probability of a particle transitioning to any other value of energy (as long as physically allowed by conservation laws). The dynamical evolution of lepton-boson distributions functions can be given by [33, 15]

$$\frac{\mathrm{d}}{\mathrm{d}t} f_e = \int_0^{+\infty} w_\chi\left(\gamma+\gamma_\gamma,\gamma_\gamma\right) f_e\left(t,\mathbf{x},\gamma+\gamma_\gamma,\mathbf{\Omega}\right)\ \mathrm{d}\gamma_\gamma - f_e(t,\mathbf{x},\gamma,\mathbf{\Omega}) \int_0^{+\infty} w_\chi\left(\gamma,\gamma_\gamma\right)\ \mathrm{d}\gamma_\gamma \tag{10}$$

$$\frac{\mathrm{d}}{\mathrm{d}t} f_\gamma = \int_1^{+\infty} w_\chi\left(\gamma+\gamma_\gamma,\gamma_\gamma\right) f_e\left(t,\mathbf{x},\gamma+\gamma_\gamma,\mathbf{\Omega}\right)\ \mathrm{d}\gamma \tag{11}$$

where $\mathbf{\Omega}$ is the velocity direction and w_χ is the rate of photon emission. Other phenomena such as Pair Production can also be added, which can reduce the photon population and increase the lepton numbers. The RHS of 10 is interpreted as a collision term in the Boltzmann equation, while the total time derivative in the LHS is the standard in the Vlasov equation.

An alternative form of these equations is

$$\frac{\mathrm{d}}{\mathrm{d}t}\begin{bmatrix} f_- \\ f_+ \\ f_\gamma \end{bmatrix} = \begin{bmatrix} \mathrm{nCS}_1 & 0 & \mathrm{nBW}_1 \\ 0 & \mathrm{nCS}_1 & \mathrm{nBW}_1 \\ \mathrm{nCS}_2 & \mathrm{nCS}_2 & \mathrm{nBW}_2 \end{bmatrix} \begin{bmatrix} f_- \\ f_+ \\ f_\gamma \end{bmatrix} \tag{12}$$

where $f_\pm$ and f_γ are the lepton and photon populations respectively, $\mathrm{nCS}_{1,2}$ and $\mathrm{nBW}_{1,2}$ are submatrices representing the rates of nonlinear Compton Scattering (photon emission) and nonlinear Breit-Wheeler (pair production). A pictorial representation of this matrix can be seen in figure 8.

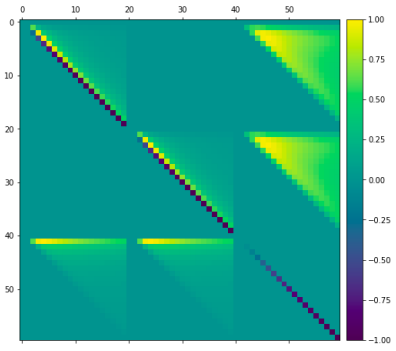

Figure 8: Matrix representation of the evolution operator in equation 12.

It can be seen that the system is linear in the distribution functions f, and can readily be put into matrix form (although nor Hermitian nor sparse). This problem could then be addressed using HHL [34] (or a variant), but as discussed previously, this approach is not suited for the NISQ era.

3. Summary and conclusions

The method described in the first part of this work allows accurate estimations of positron production in laser-electron collisions, including effects of 3D focusing geometry, spatio-temporal synchronization, and the realistic beam shape and size. This opens a possibility for fast parameter optimization, either through purely analytical calculations (if the scaling law has a simple functional form) or through numerical integration. Being much faster than full-scale PIC-QED or Monte Carlo simulations, this method can be run on a single CPU. Consequently, this allows real-time optimization and data analysis in experiments.

Other applications of the equivalent intensity distributions are possible, namely the asymptotic energy spread and divergence of the interacting electron beams, which are also imprinted on the emitted photon beams in the hard x-ray and gamma-ray range.

This analytical model could be extended to the tight-focusing regime (beyond the paraxial approximation $W_0 < 2.5\lambda$) if corrections on the effective τ and λ, and tilted interaction angle are introduced.

Additionally, in this work, we reviewed and implemented several quantum simulation techniques (in both real and simulated quantum hardware), with the long-term goal of developing algorithms to study extreme plasmas. Some methods were found more promising than others, especially in the context of applications on near-future quantum computing hardware.

In particular, we simulated the Kompaneets equation using the Carleman technique for the first time and identified potential setups within extreme plasma physics which can be transposed to quantum algorithms.

Although well established and routinely used in the scientific community, classical multidimensional nonlinear Vlasov codes are very demanding in terms of memory, which hints at the possibility of quantum codes being more efficient for specific applications. Even if it is not efficient to reconstruct entire distribution functions in a quantum computer, momenta like the average and mean-square of distributions can be easily retrieved. It is, therefore, probable that variational algorithms will play an important role in near-future applications in plasma physics.

4. Acknowledgments

I acknowledge the support from the Programme New Talents in Quantum Technologies of the Gulbenkian Foundation (Portugal) and Grupo de Lasers e Plasmas (IPFN, IST) for hosting the project.

References

[1] J. G. Kirk, A. R. Bell, and I. Arka, Plasma Physics and Controlled Fusion **51**, 085008 (2009).

[2] D. A. Uzdensky and S. Rightley, Reports on Progress in Physics **77**, 036902 (2014).

[3] R. D. Blandford and R. L. Znajek, Monthly Notices of the Royal Astronomical Society **179**, 433 (1977), https://academic.oup.com/mnras/article-pdf/179/3/433/9333653/mnras179-0433.pdf.

[4] K. Parfrey, A. Philippov, and B. Cerutti, Phys. Rev. Lett. **122**, 035101 (2019).

[5] V. I. Ritus, Journal of Soviet Laser Research **6**, 497617 (1985).

[6] T. Erber, Rev. Mod. Phys. **38**, 626 (1966).

[7] S. S. Bulanov, N. B. Narozhny, V. D. Mur, and V. S. Popov, Journal of Experimental and Theoretical Physics **102**, 9 (2006).

[8] A. R. Bell and J. G. Kirk, Phys. Rev. Lett. **101**, 200403 (2008).

[9] N. V. Elkina *et al.*, Phys. Rev. ST Accel. Beams **14**, 054401 (2011).

[10] T. Grismayer, M. Vranic, J. L. Martins, R. A. Fonseca, and L. O. Silva, Physics of Plasmas **23**, 056706 (2016), https://doi.org/10.1063/1.4950841.

[11] E. Esarey, C. B. Schroeder, and W. P. Leemans, Rev. Mod. Phys. **81**, 1229 (2009).

[12] F. Albert *et al.*, New Journal of Physics **23**, 031101 (2021).

[13] N. Neitz and A. Di Piazza, Phys. Rev. Lett. **111**, 054802 (2013).

[14] M. Vranic, T. Grismayer, R. A. Fonseca, and L. O. Silva, New Journal of Physics **18**, 073035 (2016).

[15] F. Niel, C. Riconda, F. Amiranoff, R. Duclous, and M. Grech, Phys. Rev. E **97**, 043209 (2018).

[16] C. P. Ridgers *et al.*, Journal of Plasma Physics **83**, 715830502 (2017).

[17] T. Blackburn, Plasma Physics and Controlled Fusion **57** (2015).

[18] M. Tamburini, On-shot diagnostic of electron beam-laser pulse interaction based on stochastic quantum radiation reaction, 2020, 2007.02841.

[19] T. G. Blackburn, E. Gerstmayr, S. P. D. Mangles, and M. Marklund, Phys. Rev. Accel. Beams **23**, 064001 (2020).

[20] J. M. Cole *et al.*, Phys. Rev. X **8**, 011020 (2018).

[21] K. Poder *et al.*, Phys. Rev. X **8**, 031004 (2018).

[22] S. Meuren *et al.*, On seminal hedp research opportunities enabled by colocating multi-petawatt laser with high-density electron beams, 2020, 2002.10051.

[23] H. Abramowicz *et al.*, Letter of intent for the luxe experiment, 2019, 1909.00860.

[24] O. L. Amaro and M. Vranic, New Journal of Physics (2021).

[25] J. Schwinger, Phys. Rev. **82**, 664 (1951).

[26] G. Breit and J. A. Wheeler, Phys. Rev. **46**, 1087 (1934).

[27] T. G. Blackburn, A. Ilderton, C. D. Murphy, and M. Marklund, Phys. Rev. A **96**, 022128 (2017).

[28] H. Abramowicz *et al.*, Conceptual design report for the luxe experiment, 2021, 2102.02032.

[29] Eli science and technology with ultra-intense lasers whitebook, edited by andreas thoss (2011).

[30] R. P. Feynman, International Journal of Theoretical Physics **21**, 467 (1982).

[31] J. Preskill, Quantum **2**, 79 (2018).

[32] K. Kubo, Y. O. Nakagawa, S. Endo, and S. Nagayama, Phys. Rev. A **103**, 052425 (2021).

[33] I. V. Sokolov, N. M. Naumova, J. A. Nees, and G. A. Mourou, Phys. Rev. Lett. **105**, 195005 (2010).

[34] A. W. Harrow, A. Hassidim, and S. Lloyd, Phys. Rev. Lett. **103**, 150502 (2009).